ES Energy Environ., 2022, **16**, 47-58

ES Energy & Environment

DOI: https://dx.doi.org/10.30919/esee8c666

Effect of the Wavy Leading Edge to Aerodynamic Performance Improvement in A Nuclear Steam Turbine Last Stage Blade

Fan Wu,[1] An Han,[1] Danmei Xie,[1,*] Yanan Yue[1, 2,*] and Changzhu Yang[3]

Abstract

The aerodynamic performance of a steam turbine degrades greatly when working at low load. One of the main reasons is deemed to be the flow separation. In this paper, two structures of wavy leading edge inspired in the humpback whale flipper are designed to suppress the separation: one with tubercles and one with invaginations. The sensitivity analysis of different blade heights reveals that two types of wavy leading edge bring their best enhancement under different range of negative attack angle. The design of structure adapted to the changing blade shape advances that the streamwise vortices generated by wavy leading edge can improve performance via expanding high pressure region on blades. The evolution of vortices influenced deeply by the radial velocity is much different from that in wings and aerofoils. The wheel power of turbine with the biomimetic blade is increased by 7.8% compared with the original design. The findings in our study can be used to guide the design of the steam turbine blade with better performance at low mass-flow conditions.

Keywords: Steam turbine; Biomimetic blade; Wavy leading-edge; Streamwise vortex.
Received: 25 September 2020; Revised: 18 October 2020; Accepted: 06 December 2020.
Article type: Research article.

1. Introduction

In the power generation industry, large steam turbines are required to take peak-load regulation in electrical grids.[1,2] Thus they will work at low mass-flow rate (G_m) frequently when the steam intake is less. Under such conditions, the fluid dissociation occurs and plenty of steam fluid spins within the de-flow vortex appearing along the blade pressure side, the energy of steam wasted and the working performance of steam turbines weakened. Considering the negative attack angle toward rotors at low G_m, the wavy leading edge which have been proved to upgrade the aerodynamic performance of wings and aerofoils with negative attack angle can be a useful method. Further research about whether this biomimetic blade inspired by the humpback whale flipper works on steam turbine blade successfully and how it works is necessary.

At early stages, it is noticed that the humpback whale had the ability of performing complex maneuvers with massive figure due to its flippers control function. The simulation to the flippers occurred in hydrofoils and aerofoils. Shi *et al.*[3] did numerical optimization and experimental validation for a tidal turbine blade with wavy leading-edge tubercles, imitating the humpback whales' fins. The leading edges of these types of fins had some cylindrical protrusions.[4,5] Some numerical and experimental investigations were conducted in order to understand the tubercles concept.[6-8] To study the parameters that influenced the wavy leading edge structures, Johari *et al.*[9] chose NACA (National Advisory Committee for Aeronautics) 634-021 as the basic foil, using the sinusoidal wave leading edge. After studying the influence of the wavelength and the amplitude of the wavy leading edge on the aerodynamic performance, it was found that the amplitude was the main factor to the biomimetic foil between this two parameters. Furthermore, Nierop[10] calculated the wavy leading edge pressure distribution of an infinitely long foil and concluded that the resistance of this type of blade could not increase significantly with a small angle of attack. The study also confirmed that the wavy leading edge acted like a vortex generator and that it could change the boundary layer.

The wavy leading edge with tubercles has been found to improve aerodynamic performance. Araih *et al.*[11] studied the influence of the shape and number of different leading-edge tubercles on flow. The results showed that the wave leading edge could suppress the flow separation and delay the stall. In short, the amplitude and the wavelength of tubercles were

[1] *Key Laboratory of Hydraulic Machinery Transients (MOE), School of Power and Mechanical Engineering, Wuhan University, Wuhan, Hubei, China, 430072.*
[2] *Department of Mechanical and Manufacuring Enginnering, Miami University, Oxford, OH, 45056.*
[3] *Dongfang Turbine Co., Ltd., Deyang, Sichuan, China, 618000.*
**Email:* dmxie@whu.edu.cn (D. Xie); yyue@whu.edu.cn (Y. Yue)

considered as the significant parameters. The former researches mainly found the phenomenon of de-attach flow suppression by the wavy leading edge and discussed how the two obvious parameters influenced. Some other scholars tried this structure in aerofoils.[12-14] Cai *et al*.[15,16] discussed the effect of a single leading-edge tubercles with different amplitudes on the performance of a two-dimensional aerofoil, NACA 63(4)-021, through wind tunnel experiment and theoretical analyses. They revealed that the amplitude-to-wavelength ratio played a dominant role on the performance of the modified aerofoils and the stall process of the modified airfoil with wavy leading edge was gentle and stable. The tubercle structure was also used in a hydrofoil[17] and for the reduction of aerofoil noise.[18,19] In the steam turbine blade field, Chen *et al*.[20] tried a nuclear steam turbine blade with leading-edge tubercles and confirmed that the relative internal efficiency with a biomimetic blade stage was higher than the original one.

The previous works are mostly about the wavy leading edge at a flat wing or aerofoils, they get a certain attack angle and their flow fields have little spanwise velocity. Among them, Chen *et al*.[20]firstly put this structure at a steam turbine blade. When the structure is grafted to the steam turbine blade, the tubercles should adapt to a changing attack angle because of the blade profile. Otherwise, the internal flow machinery is different from the outer flow machineries. As a rotation machinery, the steam turbine blade faces different inlet velocity angle along the different blade height (*H*), especially at low G_m. There will be many other wavy leading edge structures for adapting the changing inlet velocity angle and more parameters then just amplitude and wavelength to be optimized.

In this study, wavy leading edge structures suiting steam turbine blades is built for improving the aerodynamic performance at low G_m. To adapting the curved and twisted profile of steam turbine blades, not only the tubercle type but also the invagination type of a wavy leading edge is considered. The invagination is a new biomimetic structure constructed by the principle of building a wavy leading edge. The simulation results reveal that when putting a tubercle or an invagination on different blade height sections of the leading edge, the improvement influences of two structures are different because of the changing blade profile and the changing inlet velocity angle. Otherwise, the radial velocity of the main flow makes the streamwise vortex generated by the wavy leading edge evolve in a different way from that on the aerofoil, a kind of outer flow machinery. Then the streamwise vortex evolution and how it works on inhibiting the de-flow vortex are studied, finding that this biomimetic blade can disturb the existed de-flow vortex at low G_m and strengthen the kinetic energy exchange between main flow and blade to improve the aerodynamic performance.

2. Establishment of blade model with wavy leading edge

The last stage blade (LSB) of high-pressure (HP) rotor on a CAP1400 nuclear steam turbine is considered as the original design. Because of the periodic structure of the steam turbine passage, the fluid domain is defined as shown in Fig. 1 to save the simulation time, a single stator and rotor calculation domain. Table 1 shows several sets of calculated mass flow conditions, from 100%G_0 (design condition mass-flow rate) to 30%G_0. Among the results, the 50%G_0 flow condition approached the blower condition, for which the mechanical work of the LSB was very low, even approaching a negative value. Therefore, the 50%G_0 was chosen in this study to optimize the aerodynamic performance of steam turbine. Fig. 2 shows how a tubercle or an invagination was defined. Each tubercle or invagination was controlled by four parameters: amplitude (*A*), number (*Num*) or wavelength (*W*), thickness of the pressure side (Th_{ps}), and thickness of the suction side (Th_{ss}). The wavy structure is distributed sinusoidally on the leading edge. So the wavelength is defined firstly and the number of tubercles or invaginations (*Num*) is also determined. After that, the *A* starts at the center of each tubercle or invagination and directs along the local chord direction. To distinguish two biomimetic structure, the amplitude of an invagination is defined as a negative value toward inside the blade and when the amplitude is taken a positive value, the invaginations changes into tubercles. The Th_{ps} and Th_{ss} start from the same point as *A* and extend toward the outlet direction along the pressure side and the suction side respectively. The amplitude value is defined by the percent of the initial blade's wavelength, and the Th_{ps} and Th_{ss} values are defined by their profile lengths for the pressure or suction sides.

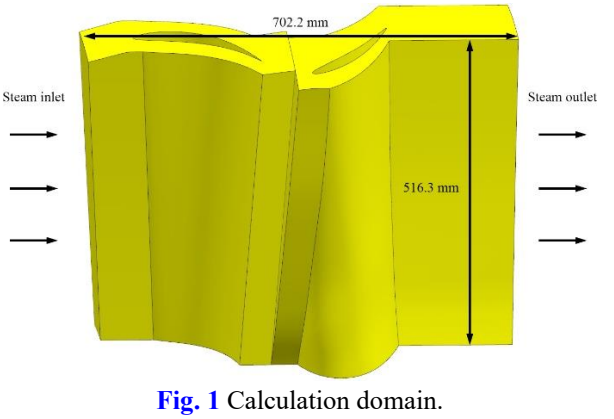

Fig. 1 Calculation domain.

The numerical model in this study is based on the Euler-Euler coordinate system. The k-epsilon formula is employed as the turbulence model, which has proven to be stable and numerically robust and has a well-established regime of predictive capability. In this turbulence model, the continuity equation is then:

$$\frac{\partial \rho}{\partial t} + \frac{\partial}{\partial x_j}\left(\rho U_j\right) = 0 \tag{1}$$

the momentum equation is:

$$\frac{\partial \rho U_i}{\partial t} + \frac{\partial}{\partial x_j}\left(\rho U_i U_j\right) = -\frac{\partial p'}{\partial x_i} + \frac{\partial}{\partial x_j}\left[\mu_{eff}\left(\frac{\partial U_i}{\partial x_j} + \frac{\partial U_j}{\partial x_i}\right)\right] + S_M \tag{2}$$

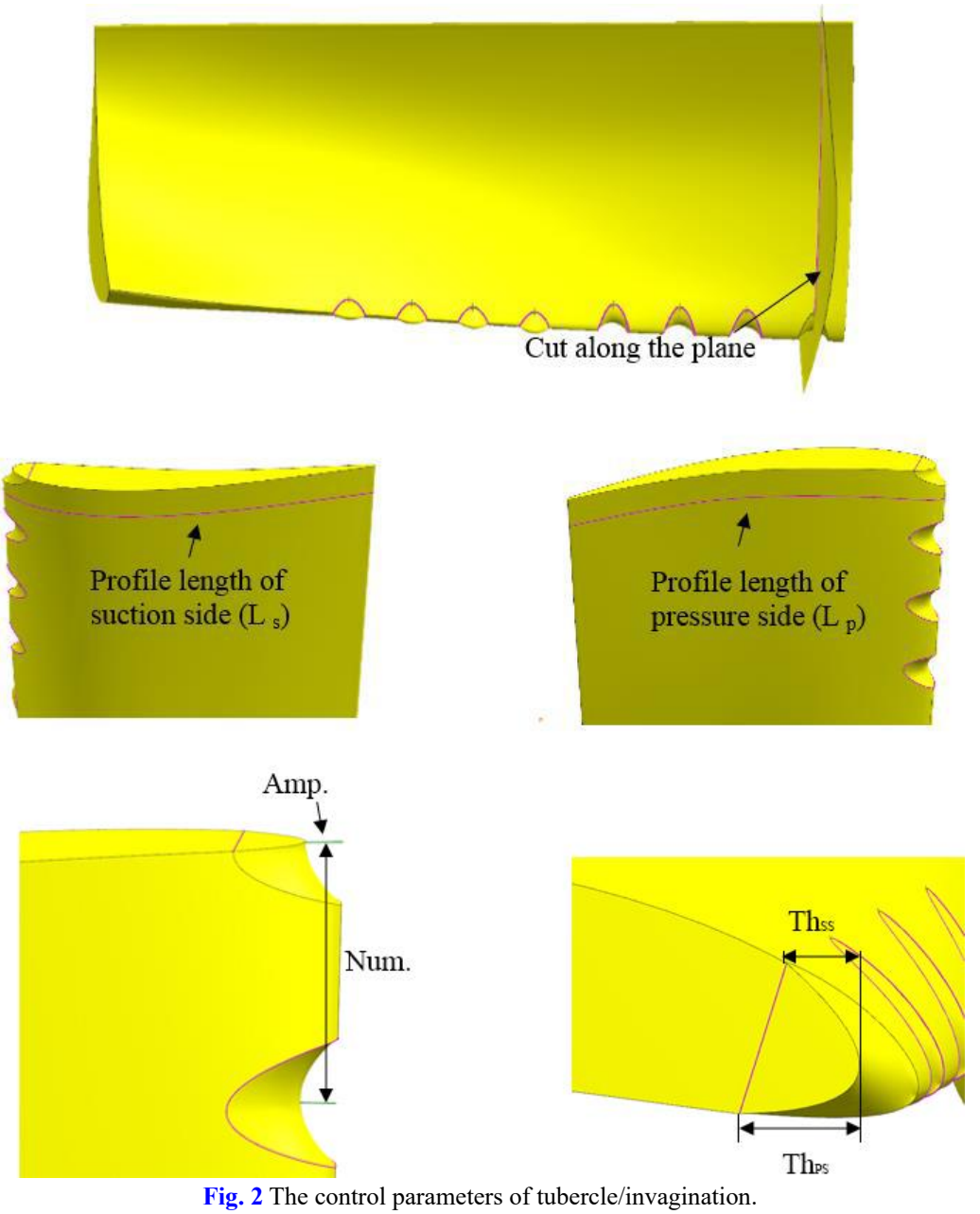

Fig. 2 The control parameters of tubercle/invagination.

Table 1. Calculation Condition Selection.

G_m	100%G_0	70%G_0	50%G_0	30%G_0
Pu of OB/kW	1870.237	677.580	110.988	-136.245

where S_M is the sum of body forces, p' is the modified pressure, defined by:

$$p' = p + \frac{2}{3}\rho k + \frac{2}{3}\mu_{eff}\frac{\partial U_k}{\partial x_k} \quad (3)$$

and μ_{eff} is the effective viscosity accounting for turbulence, defined by:

$$\mu_{eff} = \mu + \mu_t \quad (4)$$

where μ_t is the turbulence viscosity, linked to the turbulence kinetic energy k and dissipation ε via the equation:

$$\mu_t = 0.09\rho\frac{k^2}{\varepsilon} \quad (5)$$

The IAPWS IF97 material library is adopted as the gas-liquid two-phase equation of state for the working fluid. The maximum y^+ of the blade surface is below 8.65 and the average value is 1.57. Besides, the mesh average aspect ratio is 3.72 and the average orthogonal quality equals to 0.74. The boundary conditions for calculation are defined as follows: the average static outlet pressure is 1.088 MPa, the inlet mass flow is 21.63 kg s^{-1}, the inlet total temperature is 468 K, and inlet mass fraction is 0.87. In order to verify the accuracy and reliability of the above model, previous scholars' experiments are selected to verify the numerical simulation, White's L1 condition in a two-dimensional blade condensate flow test. Fig. 3 shows the two-dimensional blade, with the length of the leaf curve selected as the abscissa. It can be found in Fig. 4 that the calculation model used in this study can accurately simulate the total pressure distribution of the steam in the two-

dimensional blades, especially the strength prediction of the pressure mutation. It is proven that the steam non-equilibrium condensation in the two-dimensional blade is still simulated well by this model. Furthermore, three different numbers of meshes are built to verify the independent mesh. It can be seen in Table 2 that the numerical results show that the discrepancy of the axle direction torque (T_{or}) of the rotor blade is within 0.73% when the mesh number increases from 2.5 million to 9.5 million. Therefore, the mesh setting making number around five million is chosen. Fig. 5 shows an overview of the calculation domain mesh. The first layer mesh thickness near the blade is 0.01 mm, and there are 16 layers of inflation mesh to ensure the catch of boundary layer.

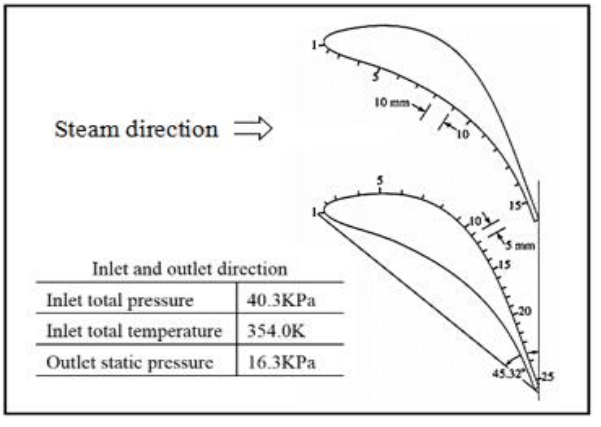

Fig. 3 Experiment conditions and geometric parameters of a two-dimensional blade.

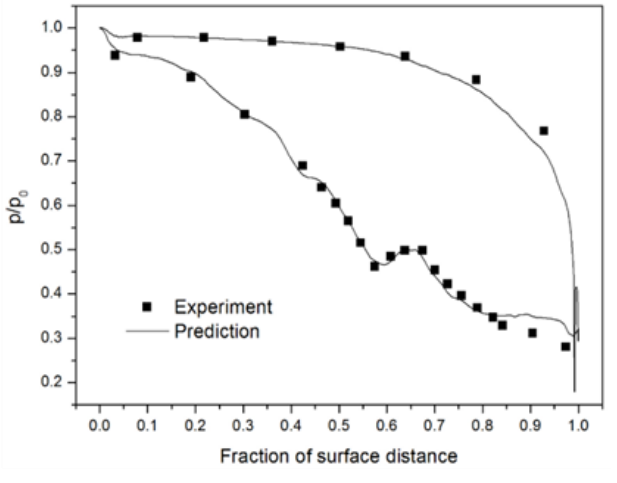

Fig. 4 Contrast of experiment and CFD results.

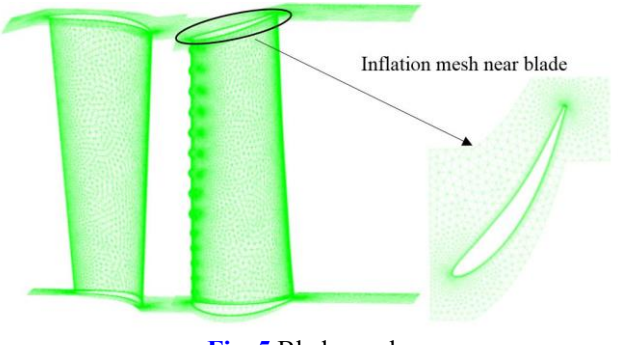

Fig. 5 Blade mesh.

Table 2. Mesh independent.

mesh numbers / million	2.5	5.0	9.5
torque / N m^{-1}	11865.7	11906.3	11819.3

3. Discussion on the sensitivity at different locations

When observing the biological prototype humpback whale fins, it is noticed that the wavy leading edge does not distribute over the whole fin. In detail, the root section of the fin remains smooth, as shown in Fig. 6. There exists a large possibility that the wavy structures in different sections of fins improves the fluid dynamic performance differently, and the wavy leading edge at the root section of the blade can play an unknown role. At the meanwhile the inlet attack angle varies a lot along the blade height H direction under low G_m. So the tubercles and invaginations are put on the tip section, middle section and root section of the LSB divided by the H to test the sensitivity at different locations. Fig. 7 shows two sets of biomimetic blade models, which are built in order to analyze the biomimetic type and location effect. To contrast the improvement of biomimetic blades, the wheel power (Pu) is defined. The Pu is controlled by the following equation:

$$Pu = T_{or} \times \omega \tag{6}$$

where the variable T_{or} is the axle direction torque, the variable ω is the angular velocity of the steam turbine, and ω is equal to 50π rad s^{-1}.

Since two sets of models are built to study the sensitivity of this biomimetic structure by comparing their acting performances via the Pu, seven cases were calculated based on a CFD platform. Starting with Fig. 8(a), it can be found that in the original blade the main flow trends toward the blade tip and the dissociation streamlines is the densest at the root section. Near the leading edge of the middle section, there exists obvious flow dissociation too but not so dense as that at root. The rotation under a low G_m takes responsibility to the radial velocity and also because of that a long strip low-pressure zone spreading from the middle section to the tip section occurs, which means the flow dissociation exists there. For C_{T1} and C_{T2}, the pressure improvement is similar whereas there is a pressure decrease after the tubercles in C_{T1} and its high-pressure zone is not as wide as that in C_{T2}. To explain that, the blade height planes on tubercle hill of two cases are drawn in Fig. 8(b). It can be deemed that the negative attack angle at the root section causes the flow to be dissociated more seriously by the tubercles. As the basic principle of wavy leading edge in references, the negative attack angle is one of the conditions under that the tubercle works. However, in this case the negative attack angle gets too large to let the tubercles become an obstacle. Furthermore, because of the rotation effect, there is less fluid at the root section than that at other sections, which leads the tubercles not to be able to generate enough of a vortex vorticity for the improve fluid. At the tip section in C_{T3}, a discontinuous high-pressure zone is observed. This phenomenon shows that the biomimetic structure effect

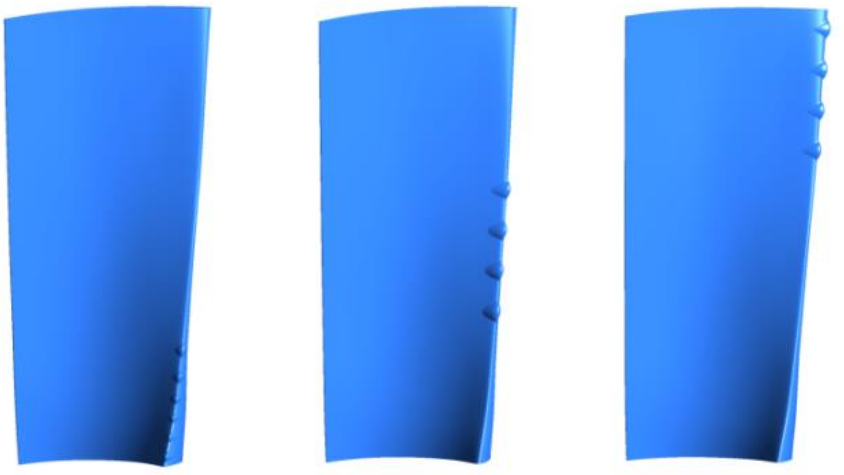

Fig. 6 Two sets of biomimetic blades. (a) Models of a biomimetic blade with tubercles. (b) Models of a biomimetic blade with invaginations.

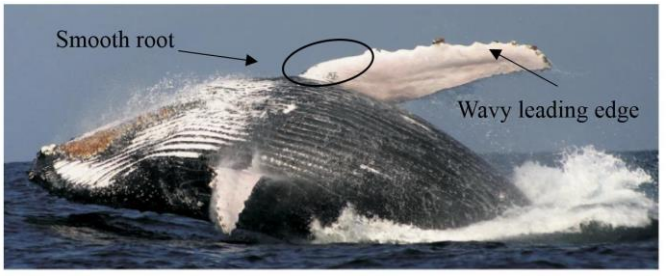

Fig. 7 Humpback whale fin.

at the tip section is unsatisfied. Such result is because the negative attack angle changes into a small value at the tip and simultaneously the tubercles make the blade thicker and squeezed the flow out so that the low-pressure zone expanded at the tip section. In general, type C_{T2} is more suitable than the other two tubercle cases. Compared to C_{I1} in Fig. 9, C_{I2} causes the middle section high-pressure zone to advance. Hence, the root section isn't a reasonable place to put biomimetic structures on. As for C_{I3}, the invaginations at the tip section does not make blade thicker and squeeze the flow out, so the generated vortex structures make sense. The Pu data is shown in Table 3 and confirms that when the G_m decreases to 50% G_0, blade C_{T2}, C_{I1}, C_{I2}, and C_{I3} have a visible rise in wheel power, which gets consistency to the rotor pressure distribution and streamlines analyses. Additionally, blade C_{T3} does not get a Pu raise, and there is even some more negative influence for blade C_{T1}. Analysis from pressure distribution and Pu perspectives illustrates that C_{T2} (tubercles at the middle section) and C_{I3} (invaginations at the tip section) can provide high pressure range improvement and Pu rise better. These are the analysis from results and how the biomimetic structure effects the flow field to improve the aerodynamic performance will be discussed in the next section.

4. Biomimetic blade influence to the passage flow field

4.1 Streamwise vortex evolution in steam turbine passage

In order to further reveal how these biomimetic structures, affect the flow field on the rotor passage, Fig. 10 of the

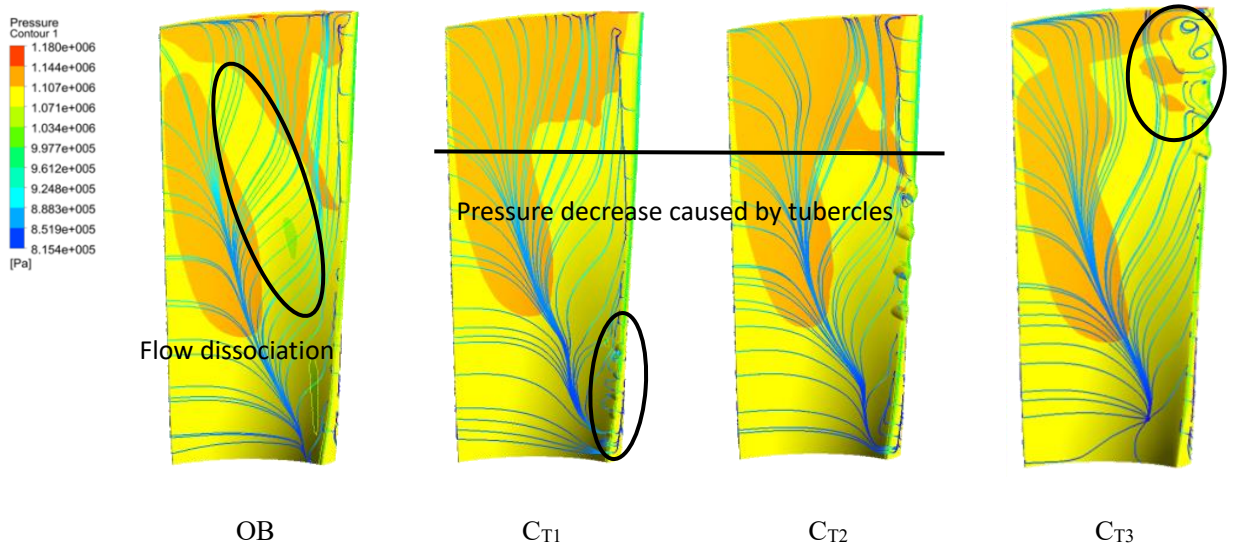

(a)

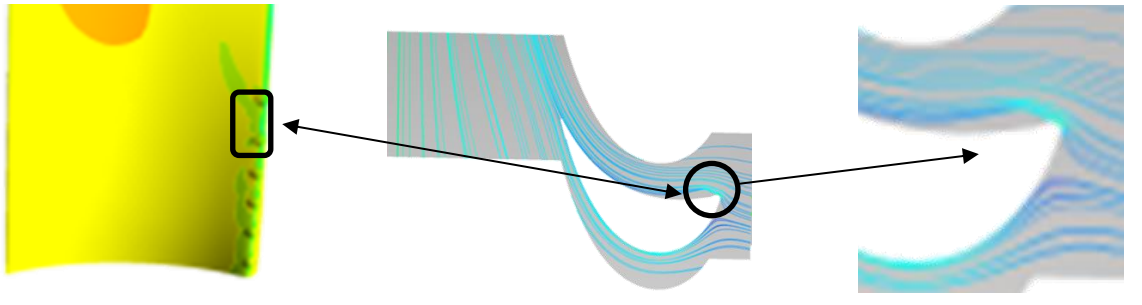

(b)

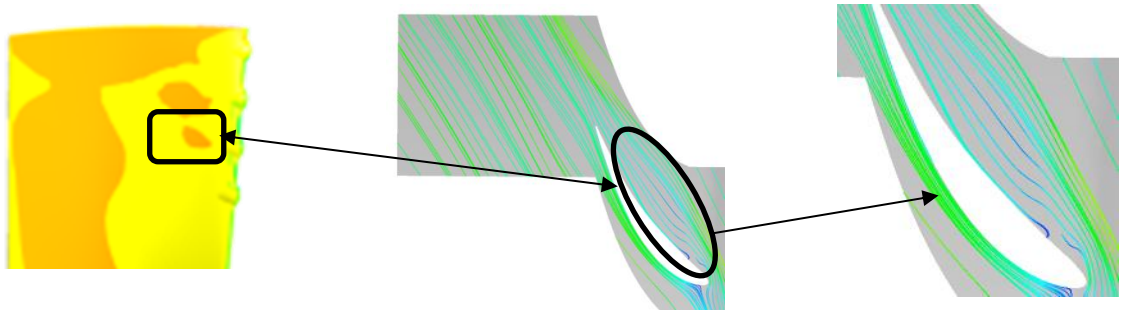

(c)

Fig. 8 Pressure contour and streamlines. (a) Pressure contribution and streamline for the rotor blade of the original blade and the t type biomimetic blades. (b) Streamlines at 0.3H plane. (c) Streamlines at 0.8H plane.

Table 3. Aerodynamic performance of the blade with a wavy leading edge at different Hs.

	Mass flow /kg s^{-1}	Torque /N m^{-1}	Pu /kW
OB	21.63	706.570	110.988
C_{T1}	21.63	661.733	103.945
C_{T2}	21.63	734.808	115.423
C_{T3}	21.63	696.880	109.466
C_{I1}	21.63	714.781	112.278
C_{I2}	21.63	726.526	114.122
C_{I3}	21.63	735.941	115.601

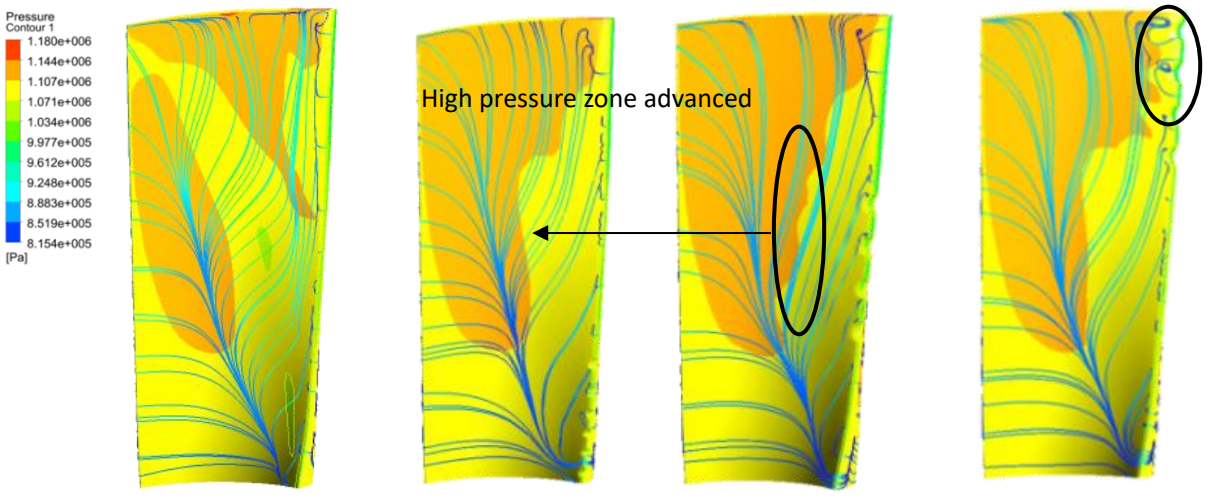

Fig. 9 Pressure contribution and streamline for the rotor blades of the CI type biomimetic blades.

streamlines starting in the mid-range before the leading edge is drawn. In this series of figures, the original blade (OB) shows the flow field problem caused by the low mass-flow condition. Firstly, the negative attack angle brings the dissociation vortex, and then because of the radial velocity the dissociation vortex turns into a kind of spiral rise vortex. It is also, the reason for a low-pressure range at the OB pressure side. Figs. 10(b) and (c) show the streamline of the C_{T2} and C_{I2}, which have the same starting point as Fig. 10(a). When the flow facing negative attack angle rushes into the tubercles, a new row of streamwise vortex is generated. In general, two tubercles will generate a vortex pair. However, there is

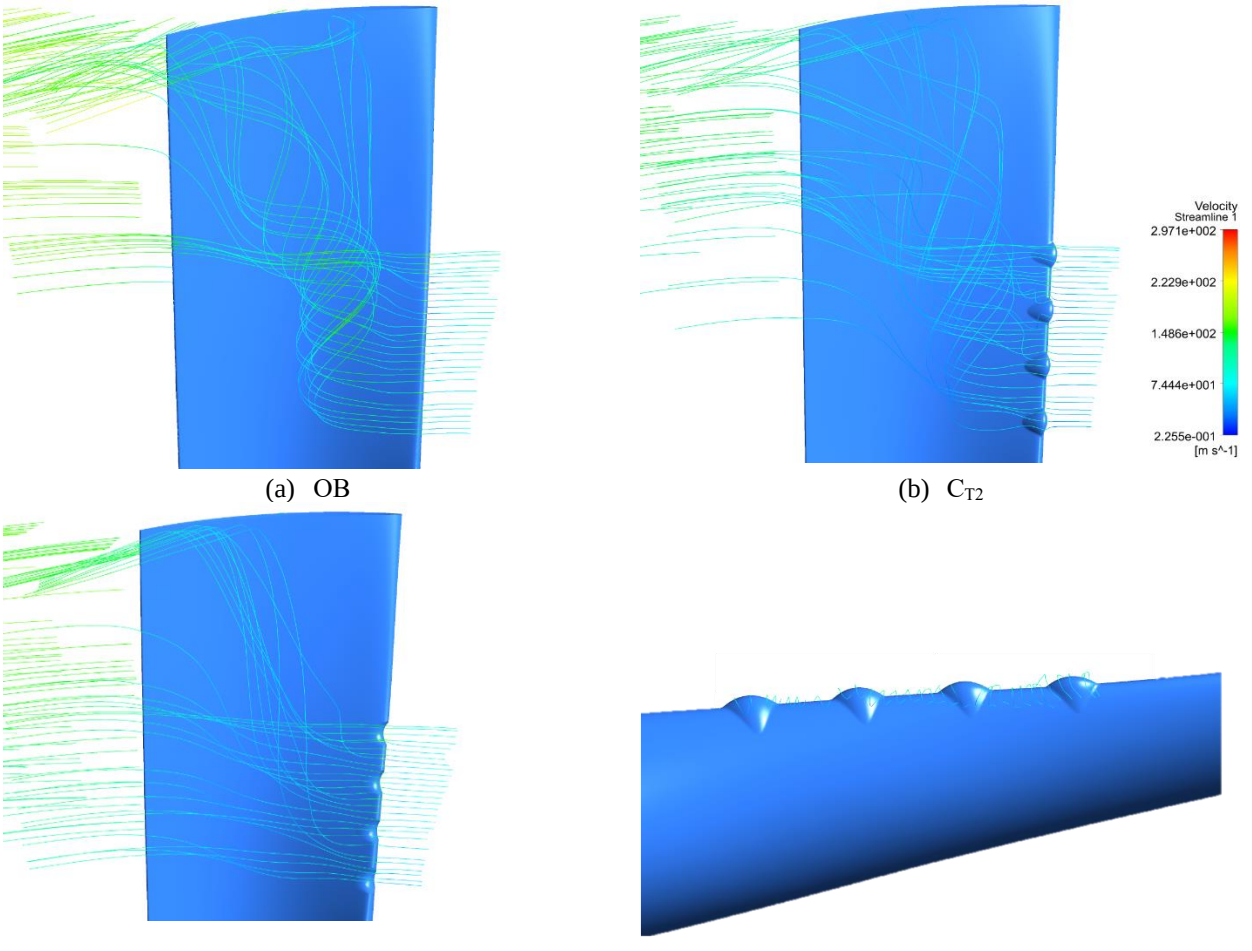

(a) OB (b) C_{T2}

(c) C_{I2} (d) C_{T2} view of streamwise

Fig. 10 Streamline contrast among OB, C_{T2} and C_{I2}. (a) OB. (b) C_{T2}. (c) C_{I2}. (d) C_{T2} view of streamwise.

streamwise vortex with only one rotation direction in the streamlines and the whole trend is flow toward the tip. The average radial velocity near the blade reaches 18.6m/s but the streamwise velocity is only 15.2 m/s. Fig. 11 plots the evolution of the vortex pair. Four section planes a-d are set in 0.07%, 0.09%, 0.11%, 0.13% of the rotor domain respectively in the direction of streamwise and the vorticity to measure the vortex intensity is controlled by the following equation:

$$Vorticity = \frac{\partial u}{\partial y} - \frac{\partial v}{\partial x} \quad (7)$$

where u is the velocity of x direction and v is the velocity of y direction.

As shown in Fig. 11, the evolution process in the internal machinery is different from that in aerofoils.[12] The vortex pairs first appear at the junctions between troughs and the tubercles above them but the other junctions between troughs and the tubercles under them only generate weak and small vortex pairs (plane a). This phenomenon will be discussed at section 4.2. At the same time, the clockwise vortex (red circles) spreads more widely than the counterclockwise vortex (blue circles). From plane a to plane b, the vortex pair evolves to the center of tubercles and the vortex grows up when the biomimetic structure as a vortex generator becomes more apparent. In the end of tubercles, plane c shows that the counterclockwise vortex is dissipating while the clockwise vortex is still growing. The reason is that the radial velocity starts to influence the vortex pairs. Near the blade surface, the velocity direction of clockwise vortex is converse to the radial velocity which gets a large magnitude. In that case, the vortex pair is one decreasing but the other increasing and that explains why the clockwise vortex distributes like a strip. When evolving to plane d, the vortex structure leaves tubercles completely so the counterclockwise vortex almost disappears. Therefore, the big radial velocity effects the streamwise vortex and suppresses one of the vortex pair rotating opposites to the radial velocity. The new streamwise vortex participates into the dissociation vortex and suppress the trend of reflow. In detail, the streamwise vortex is small and numerous and exists in the place where the main flow was originally separated. And because the streamwise vortex itself is near the blade surface, it becomes a bridge of energy exchanging between main flow and boundary layer. In the end, the dissociation vortex is suppressed and the reattach of separated flow is advanced. It is a little pity that the radial velocity of main flow can offset part of the streamwise vortex effect. For the C_{I2} streamline, the invaginations not only create a wavy leading edge to generate streamwise vortex, but also become a short groove to let the flow with negative attack angle in. The blade chord length at the trough of invaginations is actually shorter than the original. That leads to the result that the negative attack angle becomes smaller. Without a certain degree of negative angle, the de-flow vortex should be suppressed, and the energy of the flow turning into the streamwise vortex is weaker than the same situation of the tubercles. That is the flow field of mid-range, and when it comes to the tip-range, a vital change has occurred that the negative attack angle decreases. The tubercle type wavy leading edge cannot reach an excellent improvement effect when negative attack angle is too small. But the invagination type makes it up. The blade profile at tip-range is more like a plate blade, and the invaginations slightly let the flow in directly, which makes the flow fit the blade surface more. Only by that means, the streamwise vortex effect can be stronger. Considering the analyses above, a biomimetic blade that combined C_{T2} (tubercles at the middle section) and C_{I3} (invaginations at the tip section) is chosen as the initial new blade, see in Fig. 12. The simulation shows that the initial blade has 119.6 kW Pu at 50% G_m, 7.8% higher than that of the original blade.

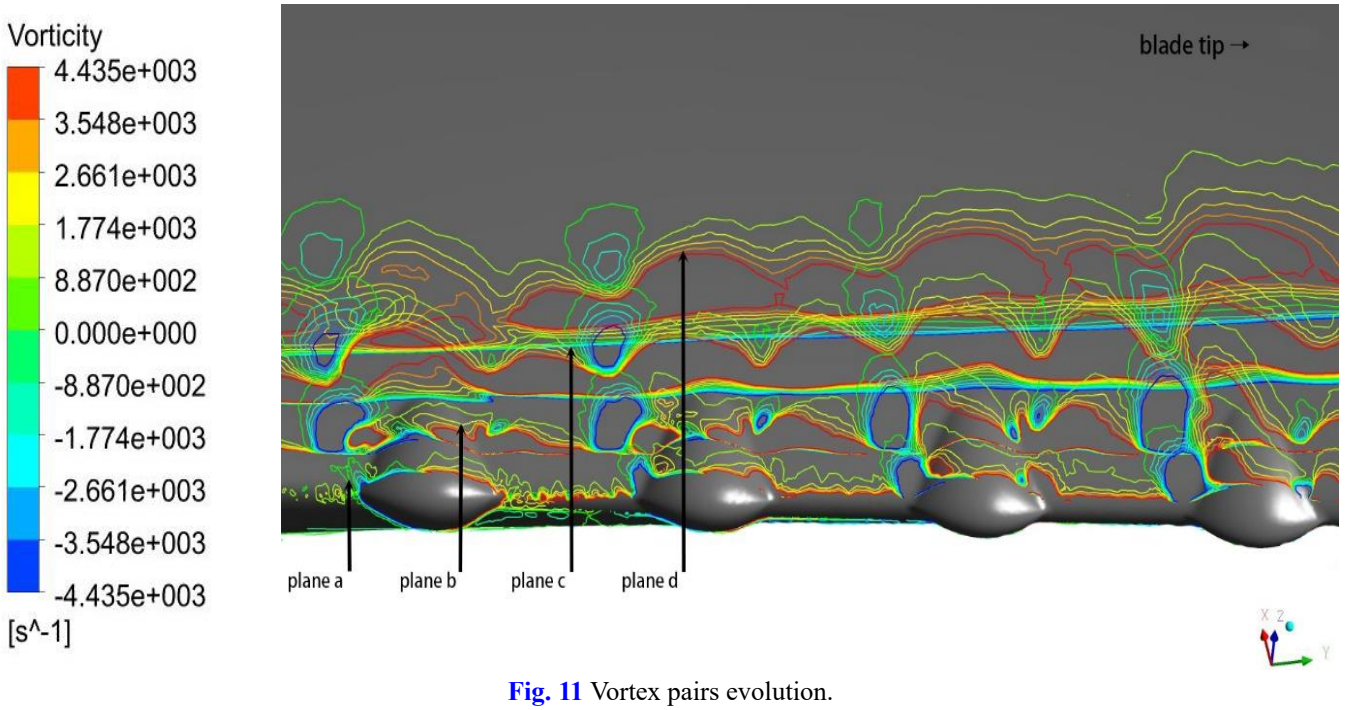

Fig. 11 Vortex pairs evolution.

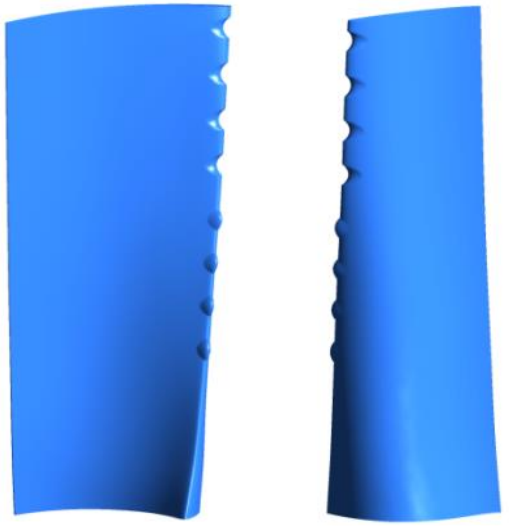

Fig. 12 Overview of final biomimetic blade.

4.2 The streamwise vortex effect on the de-flow vortex

Table 4 shows the comparison of the biomimetic blade and the original blade for different mass flow conditions. It can be seen that the biomimetic blade had a higher wheel power for all conditions, and when G_m came down, the improvement efficiency rose. Therefore, this wavy leading-edge blade will improve the aerodynamic performance of a steam turbine passage at low load condition while at the same time not influencing the design condition. The reason is that in the design condition, the blade contour at each height of the blade is built to suit the inlet steam attack angle. Without a negative attack angle, the wavy leading-edge cannot make an impact on the flow field. The streamline visualization on the original and biomimetic blade is exhibited in Fig. 13. The streamline of OB shows a consequent and neat de-flow vortex starting from the blade mid-range. Affected by the radial velocity in the whole passage, the de-flow vertex rises as a spiral. At the blade tip, there exists a second flow toward the root (Fig. 13a). Under the improvement of wavy leading-edge, the streamline of biomimetic blade gets a messier de-flow vortex and the position of de-flow vortex is closer to the leading-edge, which is the key of raising the wheel power of the blade passage. The effect of wavy leading-edge on flow field is why the de-flow vortex became messy. Fig. 11 indicates that there is streamwise vortex generated by the wavy leading-edge. However in the streamline pictures the streamwise vortex was hard to capture. That was because the two vortex (de-flow and stream direction) mixed up and both are influenced by the radial velocity. The effect of stream vortex and radial velocity is mutual. For one hand, the stream vortex is weaken and remained vortex with only one direction of rotation. In former reference[12] about wavy leading-edge putting on the aerofoils which didn't get the spanwise velocity, the stream vortex appears as pairs. But for the other hand, the average radial velocity is reduced. The average radial velocity in the streamline of Fig. 13(a) was 22.96m/s and that of Fig. 13(b) was 18.60m/s. The second flow suppression in flow field of biomimetic blade is due to the decrease of radial velocity. In short, the wavy leading-edge improves the flow situation through generating some vortex.

Table 4. Pu in different working conditions of OB and biomimetic blade.

G_m	Pu of OB/kW	Pu of biomimetic blade/kW	Increase/%
100%G_0	1870.237	1927.446	3.06
70%G_0	677.580	691.645	2.08
50%G_0	110.988	119.600	7.75
45%G_0	4.966	11.708	135.76

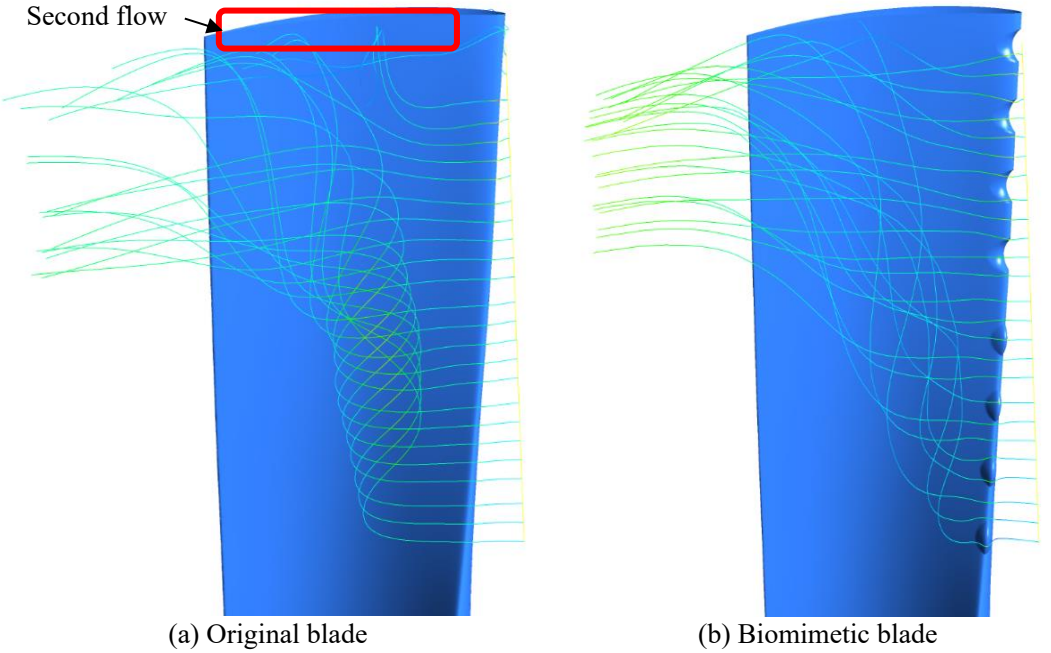

(a) Original blade (b) Biomimetic blade

Fig. 13 The construct of flow field near the blade surface between two blades.

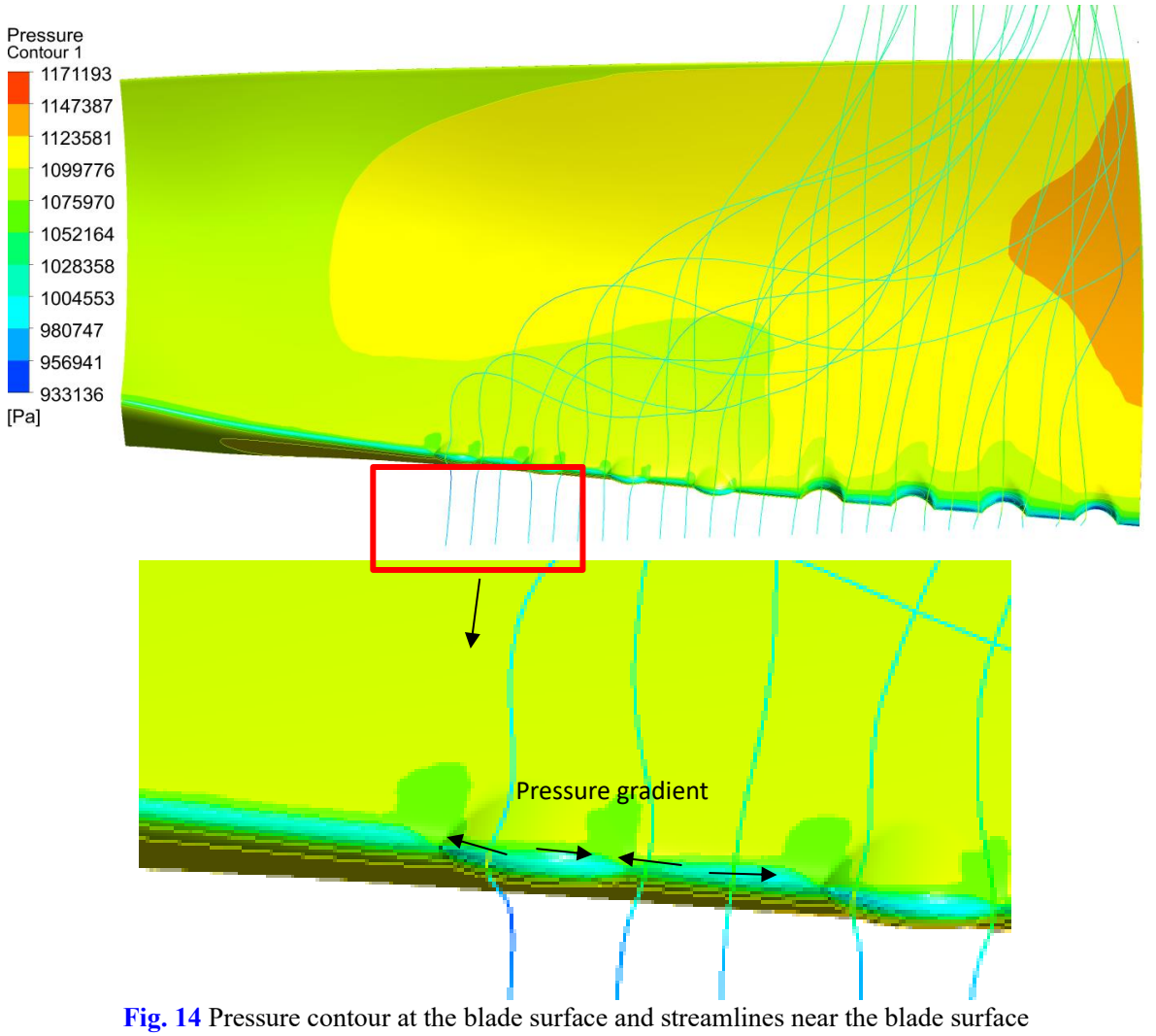

Fig. 14 Pressure contour at the blade surface and streamlines near the blade surface

Based on the sensitivity analyses, the biomimetic blade is defined as an invagination structure in the tip-range and a tubercle structure in the mid-range. In Fig. 14, the pressure distribution behind the tubercles is gradient. In detail, the junction of tubercles and blade exists the low pressure range so the steam at tubercle hill and trough flows toward the junction. Such pressure difference is the source of stream vortex. In this view, both two junctions of every trough have the motivation to generate vortex pairs but only the vortex pairs only appear on one junction. It is the radial velocity that offsets the counterclockwise vortex and the above vortex pairs blocked by tubercles remain but the under ones are greatly suppressed. In the tip-range, pressure gradient also appears behind the invaginations, wide but not so steep. The main reason is shown in Fig. 15. That is the attack angle difference. The negative degree in mid-range is larger than that in tip-range. In the part having larger negative attack angle, the tubercles can catch the kinetic energy better whereas the invaginations can reduce the flow attack on suction side while generating a certain intensity of vortex. When the available kinetic energy becomes less at a smaller negative attack angle, the invaginations should be a good choice. But there still exists a question, which is how to deal with the transition zone of tubercles and invaginations. In this work, the transition zone is built as a trough to the tubercle but a hill to the invagination. This result eventually lead to this part of blade being not used. In the follow-up work, the transition zone design will be the key point.

5. Conclusion

In this study, two kinds of structures, tubercles and invaginations of leading edge are studied based on the HP LSB of a steam turbine as an original design. The results confirm that the wavy leading-edge blade does not have to be placed at the root section which is lack of fluid. The pressure gradient on the wavy leading-edge led to the generation of stream vortex but only the clockwise one evolves normally and the counterclockwise one is suppressed by the radial velocity and disappears eventually. The stream vortex inhibits the de-flow vortex as well as decreasing the average radial velocity. The tubercles suit a larger negative attack angle whereas the invaginations suit a smaller one. The biomimetic blades get wider high pressure range than the original one in the pressure side. An optimal biomimetic blade is built by combining two structures. Its wheel power reached 119.6 kW, 7.8% higher than that of the original blade at the 50%G_0 condition.

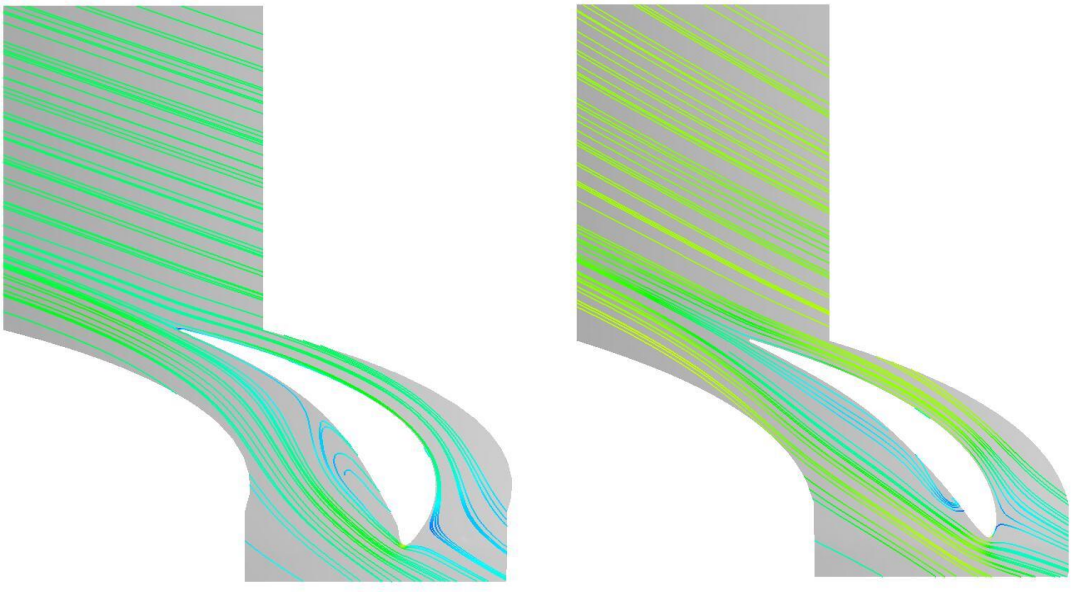

(a) Plane at 0.5H (b) Plane at 0.8H

Fig. 15 Streamline of two blade height planes.

Acknowledgments

The financial support from the National Natural Science Foundation of China (Grant No. 51776142) is acknowledged.

Conflict of Interest

There is no conflict of interest.

Supporting Information

Not applicable.

Abbreviations

A	Amplitude
W	Wavelength
Num	Numbers of Tubercle/Invagination
Th_{ps}	Thickness of Pressure Side
Th_{ss}	Thickness of Suction Side
G_m	Mass-flow Rate
G_{m0}	Design Condition Mass-flow Rate
Pu	Wheel Power of Steam Turbine
T_{or}	Axle Direction Torque
LSB	Last Stage Blade
HP	High-pressure
ω	Angular Velocity
OB	Original Blade

References

[1] G. Chen, M. Li, T. Xu, M. Liu, *Chin. Soc. Elec. Eng.*, 2017, **31**, 20-26.

[2] D. Pan, Q. Li, W. Zhang, J. Dong, F. Su, V. Murugadoss, Y. Liu, C. Liu, N. Naik, Z. Guo, *Compos. Part B*, 2021, **209**, 108609, doi: 10.1016/j.compositesb.2021.108609.

[3] W. Shi, M. Atlar, R. Norman, B. Aktas, S. Turkmen, *Renew. Energ.*, 2016, **96**, 42-55.

[4] F. E. Fish, P. W. Weber, M. M. Murray, L. E. Howle, *Integr. Comp. Biol.*, 2011, **51**, 203-213.

[5] E. Frank, J. M. B. Fish, *J. Morphol.*, 1996, **225**, 51-60.

[6] A. Corsini, G. Delibra, A. G. Sheard, *J. Fluids Eng.*, 2013, **135**, 1-9.

[7] Z. Čarija1, E. Maruši, Z. Novak, S. Fućak, *Eng. Rev.*, 2014, **34**, 93-101.

[8] C. J. Bai, W. Wang, P. W. Chen, *Int. J. Green Energy*, 2016, **13**, 1193-1200.

[9] H. Johari, C. Henoch, D. Custodio and A. Levshin, *AIAA J.*, 2007, **45**, 2634-2642.

[10] E. A. van Nierop, S. Alben, M. P. Brenner, *Phys. Rev. Lett.*, 2008, **101**, 109402.

[11] Arai H, D.Y., Nakashima T, *J. Aero Aqua Bo-Mech.*, 2010, **1**, 18-23.

[12] M. J. Kim, H. S. Yoon, J. H. Jung, H. H. Chun, D. W. Park *Comput. Fluids*, 2011, **49**, 276-289.

[13] J. Favier, A. Pinelli, U. Piomelli, *CR Mécanique*, 2012, **340**, 107-114.

[14] K. L. Hansen, N. R., R. M. Kelso, B. B. Dally, *J. Fluid. Mech.*, 2016, **788**, 730-766.

[15] C. Cai, S. Liu, Z. Zou, T. Maeda, Y. Kamada, Q. Li, R. Sato, *Phys. Fluids*, 2019, **31**, 1-16.

[16] C. Cai, Z. Zou, T. Maeda, Y. Kamada, Q. Li, K. Shimamoto, S. Liu, *Phys. Fluids*, 2017, **29**, 1-14.

[17] B. Pena, E. Muk-Pavic , G. Thomas and P. Fitzsimmons, *J. Fluid. Mech.*, 2019, **878**, 282-305.

[18] J. W. Kim, S. Haeri and P. F. Joseph, *J. Fluid. Mech.*, 2016, **792**, 526-552.

[19] P. Chaitanya P. Joseph , S. Narayanan, C. Vanderwel, J. Turner, J. W. Kim and B. Ganapathisubramani, *J. Fluid. Mech.*, 2017, **818**, 435-464.

[20] X. D. C. Tong, Y. Changzhu, Z. Hengliang, X. Yangheng, D. Haifen, Z. Jing, *Chin. Soc. Elec. Eng.*, 2018, **38**, 3605-3612.

Author information

Fan Wu *is a PhD student at School of Power and Mechanical Engineering in Wuhan University, China. His research interest includes aerodynamic performance of steam turbine.*

An Han *is a Master student at School of Power and Mechanical Engineering in Wuhan University, China. Her research interest is aerodynamic performance of steam turbine.*

Danmei Xie *is a professor at School of Power and Mechanical Engineering in Wuhan University, China. She obtained his PhD in Fluid Machinery and Engineering at Wuhan University and joined the faculty of Wuhan University in 1993. Her research interests include reliability of turbomachinery, blade design for aerodynamic performance and dehumidification.*

Yanan Yue *is a professor at School of Power and Mechanical Engineering in Wuhan University, China. He obtained his PhD in Mechanical Engineering at Iowa State University in 2011 and joined the faculty of Wuhan University in 2012. His research interest includes thermal characterization techniques at micro/nanoscale, interfacial thermal transport problems and engineering applications of heat transfer.*

Changzhu Yang *is a Senior Engineer at Dongfang Turbine Co. Ltd. in Deyang, China. His research interests includes reliability and economy of turbomachinery.*

